The Making of An Extreme Event: Putting the Pieces Together

Randall Dole[1], Martin Hoerling[1], Arun Kumar[2], Jon Eischeid[1,3], Judith Perlwitz[1,3], Xiao-Wei Quan[1,3], George Kiladis[1], Robert Webb[1], Donald Murray, Mingyue Chen[2] and Klaus Wolter[1,3]

[1]NOAA Earth System Research Laboratory, Boulder, Colorado
[2] NOAA Climate Prediction Center, Camp Springs, MD
[3] University of Colorado, Cooperative Institute for Research in Environmental Sciences, Boulder, Colorado

Submitted to *Bull. Amer. Met. Soc.*

December 10, 2012

Corresponding author address:

Martin Hoerling
NOAA/Earth System Research Laboratory
325 Broadway
Boulder CO 80305
E-mail: martin.hoerling@noaa.gov

ABSTRACT

We examine how physical factors spanning climate and weather contributed to the extreme warmth over the Central U.S. in March 2012, when daily temperature anomalies exceeded 20°C. Placing the event in a historical context, we find ~1°C warming in March temperatures since 1901. The effect of warming increased extreme heat wave probabilities. This was at least partially offset by an over 40% decline in March monthly temperature variability over the upper Midwest that reduced extreme temperature probabilities. Importantly, March 2012 had a close analogue in March 1910. The results indicate that the superposition of a strong natural variation comparable to March 1910 with a small warming trend is sufficient to account for the extreme magnitude of the March 2012 heat wave.

The proximate cause for this event was strong poleward transport of warm air from the Gulf of Mexico region, indicating the primary role of dynamical processes. These regional transports were part of a global teleconnection pattern linked to tropical forcing associated with La Niña and a strong Madden-Julian Oscillation. La Niña ocean conditions increased the probability of a Central U.S. heat wave above that contributed by the long-term warming trend. Atmospheric forcing associated with the Madden-Julian Oscillation substantially increased the probability of an extreme heat wave and provided crucial additional information beyond the trend and seasonal-interannual climate variability. We conclude that the March 2012 U.S. heat wave resulted primarily from internal climate variability, much of which was predictable, with human-induced climate change likely providing a small additional warming contribution.

1. Introduction

Nature's exuberant smashing of high temperature records in March 2012 can only be described as "Meteorological March Madness". The numbers were stunning. During much of the month, conditions more fitting of June than March prevailed east of the Rocky Mountains. For example, Chicago set daily high temperature records on nine consecutive days during 14-22 March. Eight of those days saw the mercury eclipse 80°F (26.7° C), a value not reached until late June for average daily high temperatures. The National Climatic Data Center (NCDC) reported that 2012 was the warmest March on record for the contiguous U.S. over the 118-year period since 1895, with the average temperature 8.6° F (4.8°C) above the 20th century average. At regional levels, monthly-mean anomalies were up to 16° F (9° C) above climatological normals in the core of the heat wave[1] region. In some locations, such as Marquette Michigan, daily mean temperatures were more than 40°F (22°C) above normal at the heat wave's peak. With the exceptional warmth, early blooming of trees, flowers and vegetation occurred over much of the nation east of the Rockies, with cherry blossoms reaching their peak two weeks ahead of average in Washington, DC.

What are the primary physical factors that make an event extreme, such as the event that occurred in the U.S. in March 2012? Addressing this question is fundamental to gaining scientific understanding of the causes of extreme events as well as assessing their potential

[1] The term "heat wave" is used here to indicate the exceptionally high temperatures for early spring, rather than the absolute temperatures, which in summer would be far higher, with greater potential for severe impacts.

predictability. The answers are important for applications spanning a wide range of time scales, from providing early warning of extreme weather at short lead times to informing climate adaptation strategies on longer time scales.

In this study we examine evidence for contributions from various physical factors to the March 2012 U.S. heat wave. This study follows the spirit of several recent articles in the *Bulletin of the American Meteorological Society* emphasizing the connections between climate and weather as part of a new initiative in Earth-system Prediction (e.g., Shapiro et al. 2010, Brunet et al. 2010). Here we describe how various pieces across the spectrum from climate to weather came together to produce the March 2012 extreme event.

2. Climate Overview

NCDC preliminary data indicate March 2012 had a global average temperature of 0.46° C above the twentieth century average, making 2012 the 16th warmest March on record since 1895, but also the coolest since 1999 (http://www.ncdc.noaa.gov/sotc/global/2012/3). For the global land surface temperature, NCDC's preliminary report shows March 2012 was 0.73° C above the 20th century average, the 18th warmest over the same period. Concurrent with the heat wave, below normal temperatures prevailed over large portions of the northwestern U.S., western Canada, Alaska, eastern Asia, and Australia, with warm anomalies present over Western Europe and Scandinavia (Fig. 1a). The record-setting March 2012 U.S. heat wave was thus a geographically isolated event rather than a manifestation of widespread extreme warmth.

Both the U.S. and the global surface temperature pattern during March 2012 have historical precedent, bearing a strong resemblance to conditions observed over a century earlier, in March

99 1910 (Figure 1b). Temperatures in 1910 were nearly as warm as in 2012 over the contiguous
100 U.S., with a mean departure in 1910 relative to the 20th century average of +4.5° C (compared to
101 +4.8°C in 2012). The global temperature patterns for both months, though separated by over a
102 century, are also strikingly similar. Over North America, maximum warm anomalies in March
103 1910 and March 2012 occur from the Midwest and northern Plains states northward into south-
104 central Canada, with cold anomalies further northwest over parts of western Canada and Alaska.
105 Below normal temperatures are present in both 2012 and 1910 over large portions of Eastern
106 Asia and Eastern Europe, with above normal temperatures over Western Europe. The principal
107 difference between March 2012 and March 1910 surface temperatures is in the global-mean
108 value. Compared with March 1910, the global-mean temperature in March 2012 is 0.91° C
109 warmer, consistent with a general increase in global-mean temperatures observed during the 20th
110 century that has been attributed mostly to anthropogenic causes (Solomon et al. 2007). It is
111 noteworthy that not all regions have warmed at the same rate since the beginning of the 20th
112 century. In particular, the epicenter for the March 2012 heat wave has experienced substantially
113 less temperature rise than adjacent portions of western Canada and much of Eurasia (Figure 1c).

114 A simple estimate of the event magnitude above the long-term warming trend can be obtained by
115 subtracting the temperature changes estimated from the trend since 1901 from the March 2012
116 anomalies, an approach similar to that used in previous studies (e.g., Cattiaux et al. 2010, Ouzeau
117 et al. 2011). The resulting detrended March 2012 temperature anomaly pattern is almost the same
118 as March 1910 over the central U.S. as well as many other parts of the globe (Figure 1d). Over
119 Eurasia, there is much more similarity between the detrended 2012 and 1910 patterns in areas
120 where warming trends have been large. Over parts of the U.S. most affected by the heat wave
121 there is little discernible difference between the detrended and original March 2012 patterns

because the regional trend is relatively small. Overall, this result indicates that a superposition of a strong natural variation similar to that of March 1910 on a relatively small warming trend can account for the extreme magnitude of the March 2012 heat wave.

In addition to longer-term trends, variability on seasonal-to-interannual time scales provides another important climate context for the March 2012 heat wave. The preceding winter (December-February) was characterized by La Niña conditions with below normal sea surface temperatures (SSTs) over the central and eastern tropical Pacific and above normal SSTs over Indonesia and the western tropical Pacific and central North Pacific (Fig. 2a). The corresponding time-mean outgoing longwave radiation (OLR) anomalies indicate generally suppressed convection over the central Pacific and enhanced convection from the eastern Indian Ocean to over the Maritime Continent (Fig. 2b). As such, the March 2012 U.S. heat wave occurs in the immediate aftermath of a global climate state that has been principally perturbed by a naturally occurring cooling of the tropical eastern Pacific ocean, with an overall pattern of Pacific basin-wide SSTs resembling the negative phase of the Pacific Decadal Oscillation (Mantua et al. 1997).

3. Meteorological Conditions and Associated Processes

The general timing and the maximum daily warmth associated with the March 2012 heat wave is revealed by time series of surface station observations, for which Minneapolis MN provides a representative example (Figure 3). A step-like onset of extreme warmth commences on 10 March, with temperature departures going from slightly below normal to over 11ºC (20º F) above normal in one day. The rapid onset indicates the strong role of synoptic-scale processes in the

event. Daily-mean temperature anomalies in Minneapolis reached a remarkable 20.6° C (37° F) above normal on the 17th, with three consecutive days of +20°C departures. Further east, the sudden warm spike occurs a few days later. The core period of the maximum heat wave intensity in the Midwest spans roughly12 March thru 23 March, a period for which we will present time-averaged analyses. Comparison with the 1910 time series (Fig. S1) indicates that the 1910 event had a qualitatively similar behavior, although with lower peak values and slightly longer duration.

An important feature of the heat wave is the depth of anomalously warm air through the troposphere. The time-averaged surface and 850 hPa temperature anomalies during 12-23 March (Fig. 4a and b, left) display highly similar patterns and magnitudes. Maxima exceeding +15°C occur over the Great Lakes region, with warm conditions extending across the U.S. east of the Rockies on a scale identical to the surface warmth. During this period 850 hPa vector wind anomalies were strongly southerly across a corridor of the eastern Great Plains and Midwest from Louisiana to the Canadian Prairie (Fig. 4c, left), with anomalies at times exceeding 20 m s^{1}. These flow anomalies were directed nearly straight down the time-mean temperature gradient over this region. A rough estimate of the magnitude of the poleward heat transport can be inferred from the map of wind anomalies overlain on the climatological 850-hPa temperatures (contours in Fig. 4c). The latter show approximately a 20°C mean temperature difference between the Gulf Coast and the northern Great Lakes area during March. Simple quasi-horizontal, adiabatic air mass transport would yield a roughly 20°C warming for such a displacement, a value close to the observed maximum 850 hPa temperature departures over the northern Great Lakes.

For comparison, the right panels show corresponding analyses from the 20th Century Reanalysis data set (Compo et al. 2012) for a similar 12-day period in March 1910. There is again strong similarity in the major features, although the maximum intensity is greater in 2012, largely reflecting a stronger transient peak in 2012 compared to 1910. Some of this difference may also be related to the much more limited data incorporated into the reanalysis data in 1910. The key dynamical feature evident in both years is the strong anomalous anticyclonic circulation and resulting intense poleward heat transport, with the maximum temperature anomalies occurring near the northern end of the zone of strong transport.

The surface warming was strongly coupled to poleward flow of warm air extending throughout the troposphere, as can be seen in vertical soundings over this period, such as the March 19th 00Z sounding from Chanhassen (Minneapolis, KPMX) MN (Fig. S2). The general veering of winds with increasing height is consistent with warm advection, a condition inferred also from Fig. 4c. Evidence of vertical mixing is provided by the presence of steep, near dry-adiabatic lapse rates together with wind speeds near 20 m s^{-1} just above the surface, the latter conducive to vigorous mechanical turbulence. Concerning the probable origin of the air mass depicted within this sounding, back trajectory analyses for the previous 24 hours (not shown) indicate air at 3000 m and 5000 m levels over KMPX had descended while following northeastward trajectories originating from over southern New Mexico, whereas air parcels in the boundary layer (500 m above ground level) followed quasi-horizontal trajectories originating from around eastern Texas a day earlier.

What factors were primarily responsible for producing the anomalously strong, deep and sustained southerly flow during this period? The time-mean 300-hPa height anomaly pattern for

this same 2-week period during March 2012 (Figure 6, top panel) provides an important clue. The pattern shows an arching wave train of anomalies extending northward and eastward from the western tropical Pacific, with major anticyclonic centers just east of the dateline and over the Great Lakes, the latter of which is directly related to the extreme heat wave. This pattern is consistent with what would be expected for a Rossby wave response to anomalous tropical heating (e.g., Hoskins and Karoly 1981; Plumb 1985), though such features can also arise from energy dispersion from initial perturbations located in the subtropics and mid-latitudes (e.g. Simmons et al. 1983). The time evolution of upper level circulation antecedent to and during the heat wave indicates appreciable transience, which is consistent with downstream energy dispersion from the western Pacific to North America (Fig 5, right-hand-side). In particular, strong ridge amplification occurred first over the central Pacific early in March, followed by trough deepening near the U.S. west coast, and subsequently ridge amplification over the central and eastern U.S. The latter feature is coincident with the period of most extreme heat. This evolution supports the interpretation that the U.S. heat wave was part of a larger scale dynamical phenomenon having a distinct intraseasonal time scale.

This interpretation is reinforced by satellite measurements of outgoing long wave radiation (OLR), which reveal a distinctive structure that includes enhanced convection from the Indian Ocean to the western Pacific and suppressed convection centered near 170°E just south of the equator during the first half of March (Fig. S3). The overall pattern is similar to that of the preceding winter-mean (cf. Fig. 2b), but strongly enhanced, particularly over the eastern Indian Ocean and western Maritime Continent. This enhancement is directly related to an exceptionally strong Madden-Julian Oscillation (MJO) propagating slowly eastward over this period that reinforces the winter tropical convection pattern related to La Niña (Figure 5, left-hand side).

Beginning in late February, a significant MJO was initiated over the central Indian Ocean as seen in the OLR field. A large area of negative OLR anomalies amplifies rapidly during the last week of the month and then propagates eastward at roughly 5 ms^{-1}, a typical MJO phase speed. The enhanced convective signal reaches the Maritime Continent around March 10 coincident with a suppressed convective signal just west of the dateline centered on 170E. The amplitude of this MJO event was unusually large according to the Real-Time Multivariate MJO (RMM) Index of Wheeler and Hendon (2004), exceeding two standard deviations in this index for much of the month of March. The unusually strong tropical heating anomalies extending from the Indian Ocean through the tropical western Pacific therefore provide a plausible source for forcing a Rossby wave train as seen in March 2012.

To further examine evidence for such a linkage, we have conducted experiments with a linear baroclinic model (LBM, see Peng and Whitaker 1999) forced by an idealized pattern of tropical heating anomalies resembling the general pattern observed over the Indian and western Pacific oceans and imposed on a climatological March basic state (Figure 6c). The steady solution is approximated as the average of the last five days of a 60-day integration. The observed 300 hPa height pattern (Fig. 6a) and the response of the LBM to the forcing from the tropical heating anomalies (Fig. 6b) are highly similar over the period in which the U.S. heat wave was at its peak, with a strong anticyclonic anomaly centered north of the Great Lakes. This result provides further evidence that tropical diabatic heating anomalies over the Indian Ocean and Western Pacific contributed directly to the flow anomalies that were the proximate cause for the March 2012 U.S. heat wave. These heating anomalies in turn appear to be due to the constructive superposition of convection associated with an exceptionally strong MJO event occurring on

232 subseasonal time scales with a similar seasonal convection pattern that was closely related to the
233 ongoing La Niña.
234

235 4. Anticipation

236 To what extent might a heat wave of the magnitude of the March 2012 event been anticipated
237 from prior climate conditions?
238
239 One source of potential predictability arises from long-term warming, which at global and
240 continental scales has been attributed mostly to increases in greenhouse gas concentrations
241 arising from human influences (Solomon et al. 2007). Since 1900, observed warming trends in
242 March over the heat wave region are up to 1° C (cf. Fig. 1c). Following the approach of
243 Hoerling et al. (2012), we have estimated externally forced climate trends from an ensemble of
244 20 different coupled ocean-atmosphere models used in the most recent Coupled Model
245 Intercomparison Project (CMIP5, see CLIVAR 2012). Similar to summer results presented in
246 Hoerling et al. (2012) as well as previous CMIP3 simulations (e.g., CCSP. 2008), the CMIP5
247 ensemble-mean results show warming trends over all the U.S. (Figure S4), with projected
248 temperature increases relative to the models' 1981-2010 climatologies ranging from slightly over
249 1° C in over the upper Midwest and northern Plains to less than 0.5° C over the South and near
250 the west and east coasts.
251
252 Observations and models are therefore in rough agreement in suggesting that a temperature
253 increase of approximately 1°C could be anticipated from the long-term warming trend, which in

254 the CMIP5 results is due mostly to external forcing from increasing greenhouse gas
255 concentrations. Compared to the observed peak event magnitude of approximately 20º C, a 1ºC
256 increase is small. However, even a relatively modest increase in mean temperatures would
257 increase the probability of exceeding any fixed temperature threshold, including record values,
258 and would have made the magnitude of any warm record incrementally larger. Such
259 foreknowledge would not, however, provide specific guidance as to when or where such an event
260 would occur or how intense it might be.

261 It is also possible that the variability has become larger, perhaps due to human-caused climate
262 change, thus increasing the likelihood of an extreme event. To assess this possibility, changes in
263 monthly-mean and daily variability were examined over the period 1900-2012. Fig. 7a shows a
264 time series of monthly temperature departures for Wisconsin and Minnesota, two states in the
265 epicenter of the heat wave. Visual inspection suggests that the latter part of the record has been,
266 if anything, less variable. Figure 7b provides a more quantitative evaluation by showing the
267 standard deviations of March temperatures about running 30-year means from 1900 to present.
268 Maximum variability occurs at the beginning of the record and minimum variability in 2011,
269 declining from almost 3º C early to approximately 1.7º C for the 30-year period ending in 2011, a
270 decrease of well over 40%. The change in temperature variability in this region appears fairly
271 representative of most of the U.S. (Fig. S5). Other fields, including 850 hPa heights and 850 hPa
272 winds also fail to show evidence of increasing variability (Fig. S5). Over more recent multi-
273 decadal time periods, a similar analysis for daily variability within March shows little change
274 over North America (Fig. S6). Thus, neither daily nor monthly variability show evidence of
275 increasing variability that might have increased the probability of an extreme heat wave. Indeed,

276 a decline in variability as seen in monthly means would tend to decrease that probability (Katz
277 and Brown, 1999; Sardeshmukh et al. 2000).

278 Other physical factors that may have played a role in this case include land-atmosphere
279 interactions related to anomalous snow cover. Rutgers University Global Snow Lab
280 climatological data available at http://climate.rutgers.edu/snowcover/ show that most areas of the
281 central and eastern U.S. south of a line from around Chicago to Memphis are not normally snow
282 covered in March. Thus, over much of the area experiencing record heat the absence of snow
283 cover was unlikely to explain the extreme magnitude of the event. Over the far northern U.S. and
284 Canada, the Rutgers data show near-normal snow extent at the beginning of March, with small
285 negative anomalies by March 10th. Subsequently, intense warm advection with strong southerly
286 winds resulted in rapid snow loss through melting and sublimation. Changes in the resulting
287 surface heat balance likely amplified the strong surface warming over initially snow-covered
288 regions. However, even in these areas snow cover anomalies were more a response to the heat
289 wave than the primary cause.

290 Other conditions did, however, provide early warning of the potential for an extreme heat wave
291 in the central and eastern U.S. in March 2012. Predictions from the NOAA/NCEP Climate
292 Forecast System version 2 (CFSv2; NOAA's current operational model used for seasonal and
293 subseasonal forecasts, Saha et al. 2012; Figure 8) show ensemble-averages from CFSv2
294 predictions for March 2012 initialized in December 2011, January 2012 and February 2012. The
295 December and January predictions show quite similar temperature patterns, with above normal
296 temperatures predicted over the eastern U.S. and below normal temperatures over the
297 northwestern U.S., western Canada and Alaska. This high degree of consistency largely reflects

298 the model response to SSTs on seasonal time scales, especially related to La Niña. In contrast,
299 the predictions initialized in February, while sharing several common features, also show key
300 changes from the earlier forecasts. In particular, the warmth over the U.S. intensifies
301 considerably, expands in areal coverage and shifts the epicenter of warm anomalies
302 northwestward toward the upper Midwest, much closer to the pattern observed in the following
303 month. The predicted magnitude of the ensemble-mean temperature anomalies is approximately
304 2 standardized departures of the variability in model forecasts. Other significant changes
305 between the February and earlier forecasts include marked intensification of precipitation over
306 the Maritime Continent and larger positive height anomalies with a more amplified ridge over
307 the eastern U.S. The much stronger February signal compared to earlier initializations indicates
308 that specific conditions emergent in early February, most likely in the atmospheric initial state,
309 greatly increased the probability of an extreme heat wave in March over the central and eastern
310 U.S. This additional ingredient provided crucial information beyond the trend and seasonal
311 climate conditions for the increased potential for an extreme heat wave over the central and
312 eastern U.S. in March 2012. The Climate Prediction Center capitalized on this 'forecast of
313 opportunity' to anticipate the monthly temperature pattern very well, achieving the highest skill
314 score on record for their March 2012 forecast (Heidke Skill score of +76) based on their mid-
315 February issued prediction.
316 (http://www.cpc.ncep.noaa.gov/products/predictions/long_range/tools/briefing/mon_ve
317 ri.grid.php)
318
319 The contributions from various time scales can be seen when comparing CFS ensemble forecasts
320 for March 2012 initialized from longer to shorter lead times for a large region (30N-50N, 110W-

80W) encompassing the heat wave (Fig. 9). Comparing the model climatological distribution (thick line) with the distribution of ensemble forecasts initialized 250-269 days before (thin black line), at approximately 8 to 9 months lead time there is a small shift in the distribution of about 0.5º toward warm conditions over the central U.S., but no clear evidence of an increase in the probability of warm extremes. At approximately 6 months lead time (blue curve), a larger warm signal together with an increased probability of warm extremes emerges in association with La Niña development in the coupled model predictions. This signal continues through the winter, with some further increase in the probability of warm extremes for forecasts initialized in late January (red curve). Forecasts initialized in late February (brown curve) then show a large increase in the probability of above normal temperatures and, in particular, a greatly enhanced risk of extremely warm conditions in March.

5. Putting the pieces together

The March 2012 heat wave exceeded many previous temperature records, at times by wide margins. While March 2012 was exceptional, it had historical precedent in an event that occurred over one century ago. March 1910 was nearly as extreme as in 2012, differing in contiguous U.S. temperatures by only 0.3º C. The two months also showed considerable resemblance in many features across the globe. The 1910 March heat wave originated from natural internal variability in the climate system, but was sufficiently long ago to be beyond the experience of almost all of those alive today though studies continue of that event owing to its profound relevance for wild fire management (Diaz and Swetnam 2012). This is an important reminder that individual human lifetimes (or even observational records) are often inadequate to gauge the full range of natural internal variability of weather and climate. Because of this, there

343 is a need for caution in attributing a rare event to anthropogenic causes simply because it has
344 occurred recently. Rarity alone does not imply a particular cause, and identifying the roles of
345 various factors requires careful analysis.

346 In a global context, the March 2012 heat wave was a highly localized event, occurring within an
347 overall warming climate in which the global-mean surface temperature was approximately 0.5° C
348 above the twentieth century average. Overall, we found that the superposition of a strong natural
349 variation similar to March 1910 together with a relatively small warming trend would be
350 sufficient to account for the magnitude of the March 2012 heat wave. This suggests that a
351 nonlinear response to climate change is not essential to explain the occurrence or magnitude of
352 this event.

353 The March 2012 heat wave was a transient event, occurring within a warmer than average
354 season. Daily mean temperatures reached values of 15-20° C above normal during the peak of
355 the heat wave, which extended over a period of approximately two weeks beginning in the
356 second week of March. Strong and rapid transports of warm air poleward combined with quasi-
357 adiabatic vertical mixing through a deep layer provided the proximate cause for the surface heat
358 wave. Much of the magnitude of the temperature anomalies can be reconciled with the nearly
359 horizontal transport of sensible heat from climatologically warmer regions near the Gulf of
360 Mexico poleward to north of the Canadian border. The March heat wave was therefore strongly
361 dominated by dynamical processes. This distinguishes this early spring heat wave from many
362 sustained summertime heat waves (e.g. Lyon and Dole 1995; Mueller and Senevirante 2012;
363 Hoerling et. al. 2012) where anomalous local radiative forcing and land surface feedbacks
364 associated with droughts have been shown to play first-order roles. While snow cover loss that

365 occurred in conjunction with the March 2012 event likely contributed to the magnitude of
366 warmth in the northern Midwest, much of the area affected by very high temperatures does not
367 normally have snow cover by mid-March.

368 Our results indicate that both seasonal-to-interannual and intraseasonal climate variations
369 provided important contributions to the occurrence of this extreme heat wave, with multiple
370 indications for connections to natural patterns of tropical variability. NCEP CFS model
371 ensemble predictions initialized in December and January for March 2012 consistently showed
372 an increased likelihood of warm conditions over the eastern U.S., largely as a response to
373 anomalous SSTs connected to La Niña. Predictions initialized in February had several similar
374 features, but also key differences, indicating a large increase in the probability for an
375 exceptionally warm March over the central and eastern U.S. This provided evidence that
376 specific conditions emergent in early February, most likely in the atmospheric initial state,
377 played a critical role. Observational and model results showed that the development of an
378 exceptionally strong MJO in February was of central importance, forcing an extratropical wave
379 train very similar to the observed circulation anomalies during the period in which the heat wave
380 was most extreme. This MJO provided a crucial extra ingredient on intraseasonal time scales that
381 substantially increased the likelihood of an extreme heat wave over the central and eastern U.S.
382 and Canada during March 2012, and also is an example of the bridging between weather and
383 climate (Zhang, 2012).

384 We also found that monthly temperature variability has declined substantially since the
385 beginning of the twentieth century in parts of the upper Midwest affected by the heat wave. Such
386 a decline has important implications. It would lead to an expectation for fewer extreme events

387 rather than more. In particular, declining variability would lead to a lower probability of warm
388 extremes compared to what would be expected from a mean warming trend alone. Thus,
389 estimates of changes in the probability of extreme events based on the mean trend alone may
390 contain significant errors, with a bias toward overestimation of warm extremes. The large trend
391 in the monthly temperature variability over the twentieth century also indicates that 30-year
392 periods are likely too short to obtain reliable climatological estimates of monthly-mean variance.
393 Therefore, estimated frequencies of monthly or seasonal extremes based on the mean and
394 variance of 30-year periods (e.g., Hansen et al. 2012) should be interpreted with great caution.

395 Fig. 10 illustrates schematically how multiple pieces from longer-term climate trends to shorter-
396 term weather and climate variations came together to produce the extreme March heat wave,
397 based on a synthesis of observational results, CMIP5 projections and CFSv2 predictions
398 presented in this study. A long-term warming trend led to a modest increase in March mean
399 temperatures, shifting the temperature probability distribution a small distance to the right (solid
400 red curve) from the climatological distribution (thick blue curve). Such a shift would increase the
401 likelihood of an extreme heat wave. The addition of specific boundary conditions for 2011-
402 2012, especially related to La Niña, increased this probability further (dashed pink curve). The
403 large shift in early February associated with an MJO event (thin blue curve) provided crucial
404 information beyond the trend and seasonal climate conditions that indicated a greatly increased
405 potential for an extremely warm March. Thus, several pieces from climate to weather ultimately
406 linked together favorably to make the observed March 2012 heat wave. However, even at
407 shorter lead times the heat wave was far from certain. As the width of the distributions indicates,
408 a large range of outcomes was possible, and what occurred could well have been otherwise.

409 Overall, our results indicate that the magnitude of the March 2012 heat wave can be largely
410 explained by natural variability, with an additional modest contribution from a long-term
411 warming trend that is likely due mostly to human influences. Phenomena across the temporal
412 spectrum from climate change to weather all contributed to making this event extreme.

413 Increasing understanding of the linkages between weather and climate, and especially the
414 implications for anticipating future extreme events, will be essential for meeting many societal
415 needs, from improving early warning on potential disasters to providing information needed for
416 longer-term adaptation to a changing climate. Toward this end, large ensembles developed for
417 climate change projections and initialized weather and climate predictions, as used in this study,
418 have become increasingly useful for identifying how pieces across the spectrum from climate to
419 weather fit together in order to better understand and anticipate extreme events. While advances
420 have been impressive, there remain major opportunities for future progress (Shapiro et al. 2010).
421 We still have much to learn.

422

References

Brunet, Gilbert, and Coauthors, 2010: Collaboration of the Weather and Climate Communities to Advance Subseasonal-to-Seasonal Prediction. *Bull. Amer. Meteor. Soc.*, **91**, 1397–1406.

Cattiaux J, R. Vautard, C. Cassou, P. Yiou, V. Masson-Delmotte, and F. Codron, 2010: Winter 2010 in Europe: a cold extreme in a warming climate. *Geophys. Res. Lett.,* 3**7**, pp. L20704. doi:10.1029/ 2010GL044613.

CCSP, 2008: *Reanalysis of Historical Climate Data for Key Atmospheric Features: Implications for Attribution of Causes of Observed Change*. A Report by the U.S. Climate Change Science Program and the Subcommittee on Global Change Research [Randall Dole, Martin Hoerling and Siegfried Schubert (eds.)]. NOAA, NCDC, Asheville, NC, 156 pp.

CLIVAR, 2012. WCRP Coupled Model Intercomparison Project – Phase 5. Special Issue of the *CLIVAR Exchanges Newsletter,* No. 56, Vol. 15, No. 2

Compo and Coauthors, 2011: The Twentieth Century Reanalysis Project. *Quarterly J. Roy. Meteorol. Soc.*, **137**, 1-28. DOI: 10.1002/qj.776.

Diaz, H. F. and T. W. Swetnam, 2012: The Wildfires of 1910: Climatology of an extreme early 20th Century event and comparison with more recent extremes. *Bull. Amer. Met. Soc.* (submitted).

Hansen, J., M. Sato, and R. Ruedy, 2012: Perception of climate change. *Proc. Natl. Acad. Sci.*, **109**, 14726-14727

Hoerling, M., A. Kumar, R. Dole, J.W. Nielsen-Gammon, J. Eischeid, J. Perlwitz, X.W. Quan, T. Zhang, P. Pegion, M. Chen 2012: Anatomy of an Extreme Event. *J. Climate* doi: http://dx.doi.org/10.1175/JCLI-D-12-00270.1

Hoskins, B. J., and D. J. Karoly, 1981: The Steady Linear Response of a Spherical Atmosphere to Thermal and Orographic Forcing. *J. Atmos. Sci.*, **38**, 1179–1196.

Kalnay, E., and coauthors, 1996: The NCEP/NCAR 40-year reanalysis project, *Bull. Amer. Meteor. Soc.,* 77, 437-470

Katz, R.W., and B. G. Brown, 1999: Extreme events in a changing climate: variability is more important than averages. *Climate Change*, **21**, 289-302.

Liebmann B. and C.A. Smith, 1996: Description of a Complete (Interpolated) Outgoing Longwave Radiation Dataset. *B. Amer. Meteor. Soc.*, **77**, 1275-1277.

Lyon, B. and R. M. Dole, 1995: A Diagnostic Comparison of the 1980 and 1988 U.S. Summer Heat Wave-Droughts. *J. Climate*, **8**, 1658–1675.

Mantua, N. J., S. R. Hare, Y. Zhang, J. M. Wallace, and R. C. Francis, 1997: A Pacific Interdecadal Climate Oscillation with Impacts on Salmon Production. *Bull. Amer. Meteor. Soc.*, **78**, 1069–1079.

Mueller, B. and S. I. Seneviratne, 2012: Hot days induced by precipitation deficits at the global scale. *Proc. Natl. Acad. Sci.,* **109**, 12398-12403

Ouzeau, G., J. Cattiaux, H. Douville, A. Ribes, and D. Saint-Martin (2011), European cold winter 2009-2010: How unusual in the instrumental record and how reproducible in the Arpege-Climate model? *Geophys. Res. Lett*, **38**, pp. L11706. doi:10.1029/2011GL047667

Peng, S., and J. S. Whitaker, 1999: Mechanisms Determining the Atmospheric Response to Midlatitude SST Anomalies. *J. Climate*, **12**, 1393–1408.

Plumb, R. A., 1985: On the Three-Dimensional Propagation of Stationary Waves. *J. Atmos. Sci.*, **42**, 217–229.

Sardeshmukh, P. D., G. P. Compo, M.C. Penland, 2000: Changes of Probability Associated with El Niño. *J. Climate*, **13**, 4268–4286.

Shapiro, M., and coauthors, 2010: An Earth-System Prediction Initiative for the Twenty-First Century. *Bull. Amer. Meteor. Soc.*, **91**, 1377–1388.

Simmons, A.J., J. M. Wallace and G. W. Branstator, 1983: Barotropic wave-propagation and instability, and atmospheric teleconnection patterns. *J. Atmos. Sci*., **40**, 1363-1392.

492 Smith, T.M., R. W. Reynolds, T. C. Peterson, and J. Lawrimore, 2008: Improvements to
493 NOAA's historical merged land-ocean surface temperature analysis (1880-2006). J. Climate, 21,
494 2283-2296.
495
496 Solomon, S., and Coauthors, 2007: Technical Summary. In: *Climate Change 2007: The Physical*
497 *Science Basis*. *Contribution of Working Group I to the Fourth Assessment Report of the*
498 *Intergovernmental Panel on Climate Change* [Solomon, S., D. Qin, M. Manning, Z. Chen, M.
499 Marquis, K.B. Averyt, M. Ignore and H.L. Miller (eds.)]. Cambridge University Press,
500 Cambridge, United Kingdom and New York, NY, USA.

501 Wheeler, M. and H. Hendon, 2004: An all-season real-time multivariate MJO index:
502 Development of an index for monitoring and prediction. *Mon. Wea. Rev.*, **132**, 1917-1932.

503 Zhang, C., 2012: Madden-Julian Oscillation: Bridging weather and climate. *Bull. Amer. Met. Soc.*
504 (submitted).
505

506

507

508

Appendix 1: Linear Baroclinic Model

The linear baroclinic model (LBM) is a time-dependent atmospheric model based on the primitive equations. The model consists of five basic equations describing vorticity, divergence, temperature, mass, and hydrostatic balances. The model is global with a T21 spherical harmonic horizontal resolution and 10 equally spaced pressure levels. There is no topography at the lower boundary. The model is linearized about a three-dimensional time-mean March basic state over 1981-2010 and forced by a couplet of diabatic heating with a positive maximum centered at (5S 100E) and negative maximum at (5S 170E), which is designed to mimic the anomalous rainfall pattern observed over the Indian Ocean and western Pacific Ocean during the first half of March 2012. Additional experiments indicate that the results are not sensitive to the precise choice of locations of the maxima within the same general regions described above.

The specified heating anomalies have maximum values of 2.5 K day^{-1} at 350 hPa. Perturbations from the basic state are interpreted as the linear model response to the specified forcing. Rayleigh friction and Newtonian damping are given the rate of $(1\ day)^{-1}$ at the lowest level, decreasing linearly to zero at 700 hPa. A biharmonic diffusion with a coefficient of $2 \times 10^{16}\ m^4\ s^{-1}$ is applied in the vorticity, divergence, and thermodynamic equations. These levels of dissipation are sufficient to stabilize the model so that a steady state can be reached. A thermal diffusion with a coefficient of $2 \times 10^6\ m^2\ s^{-1}$ is added to represent the eddy effects. We approximate the steady solution as the average of the last 5 days of a 60-day integration.

Figure Captions

Figure 1. March surface temperature anomalies for a) 2012 and b) 1910. c) March temperature change derived from the trend over the 111-year period 1901-2011. d) Detrended March 2012 temperature anomalies. (Units: ºC). Areas of insufficient data are indicated by stippling. Data are from the NCDC merged land-ocean dataset Version 3b (Smith et al. 2008). Anomalies are departures from means over a 1981-2010 base period unless stated otherwise.

Figure 2. For the winter (December-February) preceding March 2012, the time-mean a) SST anomalies (ºC) and b) OLR anomalies (Wm^{-2}). The SSTs are from NOAA OI SST v2 (Reynolds et al. 2002) and the OLR from the NOAA Interpolated OLR data set (Liebmann and Smith 1996).

Figure 3. Daily-average temperatures (top), daily departures (middle), and maximum and minimum temperatures (bottom) for Minneapolis, MN for February to April 2012 (ºC). Temperature data are from the Global Daily Climatology Network.

Figure 4. Left side panels: 12-23 March 2012 time-mean a) Surface temperature anomalies (ºC), b) 850 hPa temperature anomalies (ºC), and 850 hPa vector wind anomalies together with March climatological-mean 850 hPa temperatures (ºC). The right side panels show corresponding maps for 18-29 March 1910. Data for 2012 are derived from the NCEP/NCAR Reanalysis (Kalnay et al. 1996), and for 1910 from the 20th Century Reanalysis Project (Compo et al. 2011).

Figure 5. Time-longitude analyses over the period February 1- April 30 2012 of a) OLR anomalies (W m^{-2}) averaged over 5ºN-5ºS extending from West Africa to the east-central Pacific

555 and b) 300 hPa height anomalies (m) for a mid-latitude band (30-50° N) from East Asia to the
556 eastern North Atlantic. The sloped dash lines depict (a) the eastward propagating MJO
557 convective signal, and (b) downstream energy dispersion from the Pacific to the North Atlantic.
558
559 Figure 6. Comparison between observed 300 hPa height anomalies and the response of a Linear
560 Baroclinic Model (LBM) to forcing from tropical diabatic heating anomalies similar to those
561 observed in early March 2012. (a) March 12-23 time-mean 300 hPa height anomalies (m). (b)
562 LBM response to anomalous tropical forcing (m). (c) Idealized diabatic heating pattern used to
563 force the LBM. For further details on the LBM, see Appendix 1.
564
565 Figure 7. Minnesota-Wisconsin area-average a) March temperature anomaly time series from
566 1900 to 2012, along with 30-year running mean of this average plotted at the ending year, and b)
567 the standard deviation of the March area-average temperatures about their 30-year running
568 means, plotted at the ending year (°C). The asterisks denote the corresponding values for the 30-
569 year periods ending in 2012, illustrating how inclusion of March 2012 alters the statistics. From
570 NCDC Climate Division data. Asterisks denote the values of the 30-year mean and standard
571 deviation for 1983-2012.
572
573 Figure 8. Operational ensemble mean CFSv2 forecasts verifying March 2012 based on
574 initializations during (left) December 12-21 2011, (middle) January 12-12 2012, and (right)
575 February 1-10 2012. Predictions are for (top) surface temperature anomalies (first interval 0.5°C,
576 1°C intervals thereafter; warm (cold) anomalies in red (blue)), (second row) 200 hPa heights
577 (total field contoured, anomalies shaded every 15m; positive (negative) anomalies in red (blue)),

578 (third row) precipitation anomalies (first interval 1mm/day, 2mm/day intervals thereafter; wet
579 (dry) anomalies in green (red)), and (bottom) sea temperature anomalies (intervals are 0.25, 0.5,
580 1.0, and 2.0 °C; warm (cold) anomalies in red (blue)). Predictions are made four-times daily,
581 yielding a 40-member ensemble for each 10-day period. All anomalies are defined relative to
582 CFSv2 lead-time dependent March hindcast climatologies for 1982-2010.
583
584 Figure 9. The PDFs of 2-meter air temperature monthly anomalies for March 2012 derived from
585 CFSv2 model predictions at different lead times (thin curves) and for a March climatological
586 distribution of hindcasts (thick black curve). All prediction PDFs are derived from 80-member
587 ensembles, while the climatological PDF is derived from all March hindcasts (retrospective
588 forecasts) up to 6 months in advance over the years 1999-2010 (1728 members). Anomalies are
589 defined relative to the CFSv2 hindcast climatologies for 1982-2010 as in Figure 8. Predictions
590 are averaged for the region 30N-50N, 110W-80W.
591
592 Figure 10. A schematic representation of how predictions for the March 2012 PDF shifted away
593 from the climatological distribution (blue) in response to different factors. These include multi-
594 decadal variations and trends operating on time scales well beyond a season (red), SSTs and
595 other boundary forcings on seasonal time scales (dashed), and the MJO and other phenomena
596 dominated by atmospheric processes on subseasonal-to-daily time scales.
597
598 Figure S1. As in Figure 3 for Minneapolis, Minnesota temperature time series for Feb-April
599 1910.
600

601 Figure S2. Radiosonde data from the surface to 100 hPa of temperatures and dewpoints (ºC) and
602 winds for Chanhassen (Minneapolis, MPX) on March 19 2012 00Z.
603
604 Figure S3. Time-mean OLR over March 1-15 2012 (W m^{-2}). Data source as in Figure 2.
605
606 Figure S4. CMIP5 ensemble average of predicted March 2012 temperatures anomalies (in ºC
607 relative to model 1981-2010 climatology).
608
609 Figure S5. Standard deviation of monthly March 850 hPa temperature (top), 850 hPa
610 geopotential height (middle) and 850 hPa meridional wind speed (bottom) over the base period
611 1961-1990 (left) and the ratio of standard deviations for 1991-2011 relative to 1961-1990 (right).
612 [Data source: NCEP/NCAR reanalysis].
613
614 Figure S6. As in Supplementary Figure 5 but for standard deviations of daily temperatures in
615 March (left) for 1961-90 and the ratio of standard deviations for 1991-2011 relative to 1961-90
616 (right). Contour intervals for the 1961-1990 base period (left panels) are doubled relative to
617 monthly values in Figure S5.
618

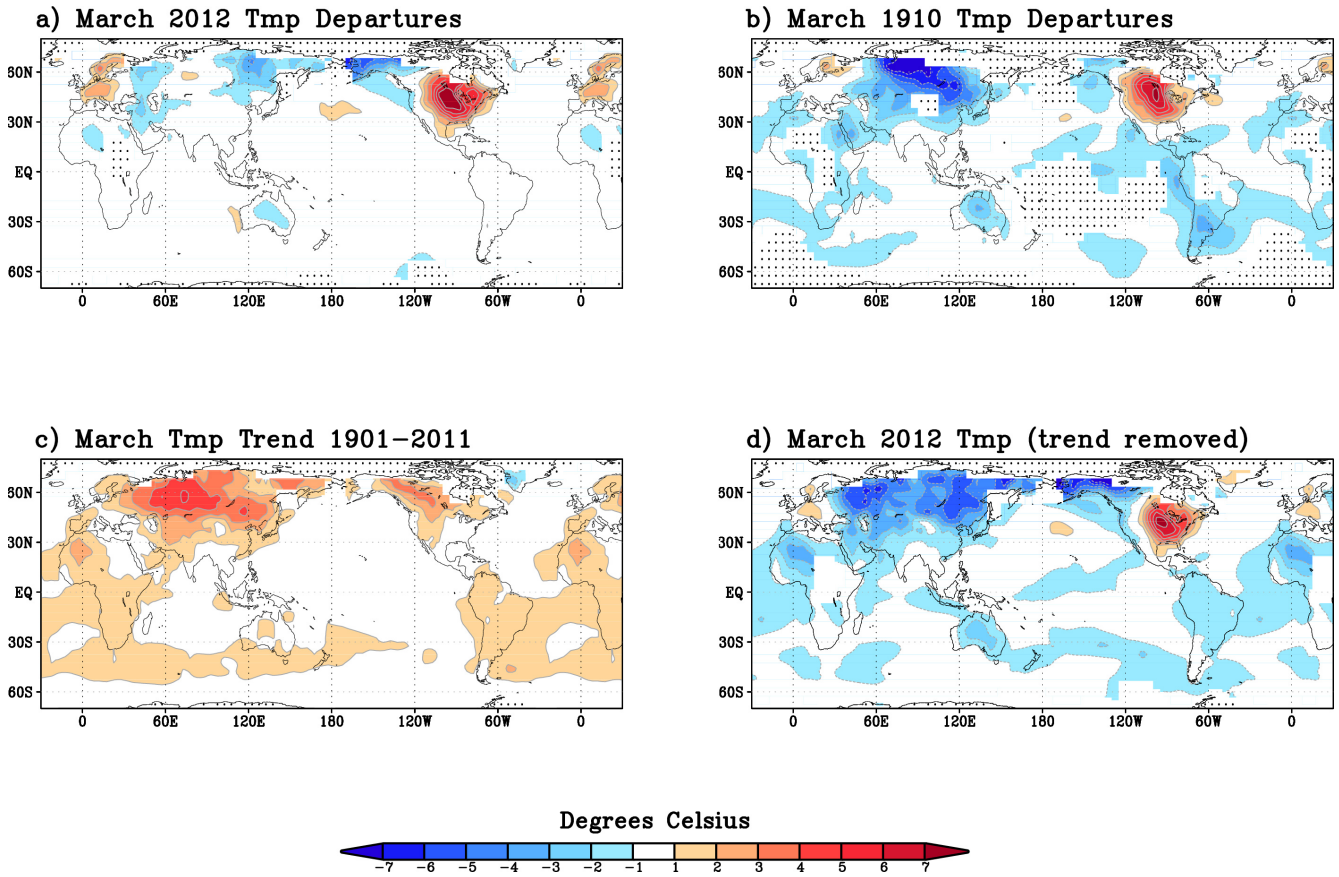

Figure 1. March surface temperature anomalies for a) 2012 and b) 1910. c) March temperature change derived from the trend over the 111-year period 1901-2011. d) Detrended March 2012 temperature anomalies. (Units: ºC). Areas of insufficient data are indicated by stippling. Data are from the NCDC merged land-ocean dataset Version 3b (Smith et al. 2008). Anomalies are departures from means over a 1981-2010 base period unless stated otherwise.

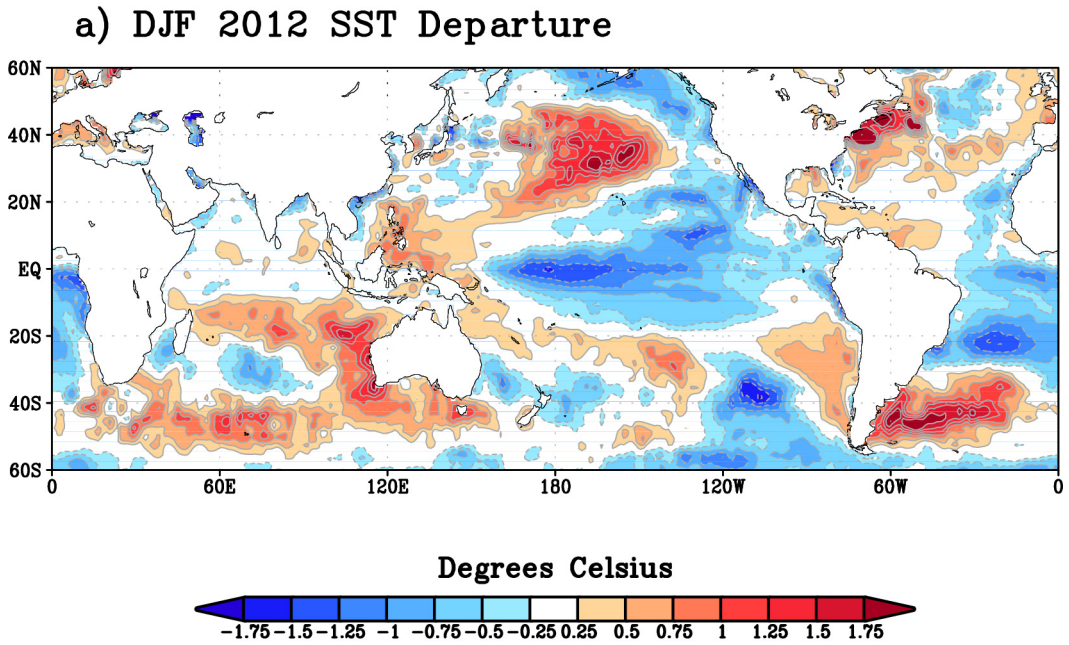

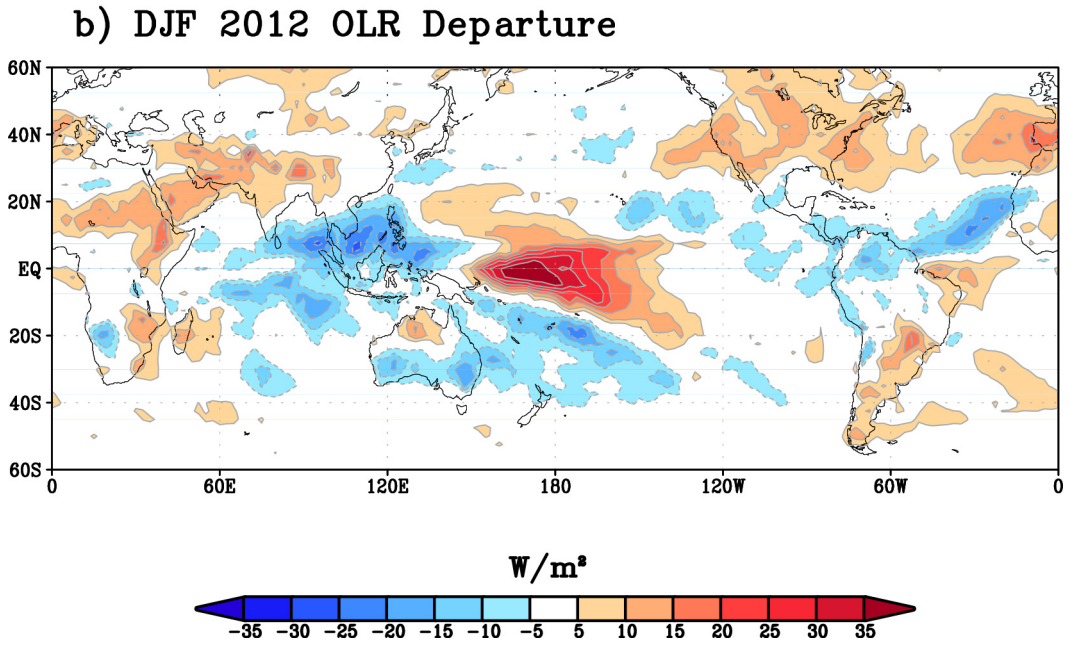

Figure 2. For the winter (December-February) preceding March 2012, the time-mean a) SST anomalies (ºC) and b) OLR anomalies (Wm^{-2}). The SSTs are from NOAA OI SST v2 (Reynolds et al. 2002) and the OLR from the NOAA Interpolated OLR data set (Liebmann and Smith 1996).

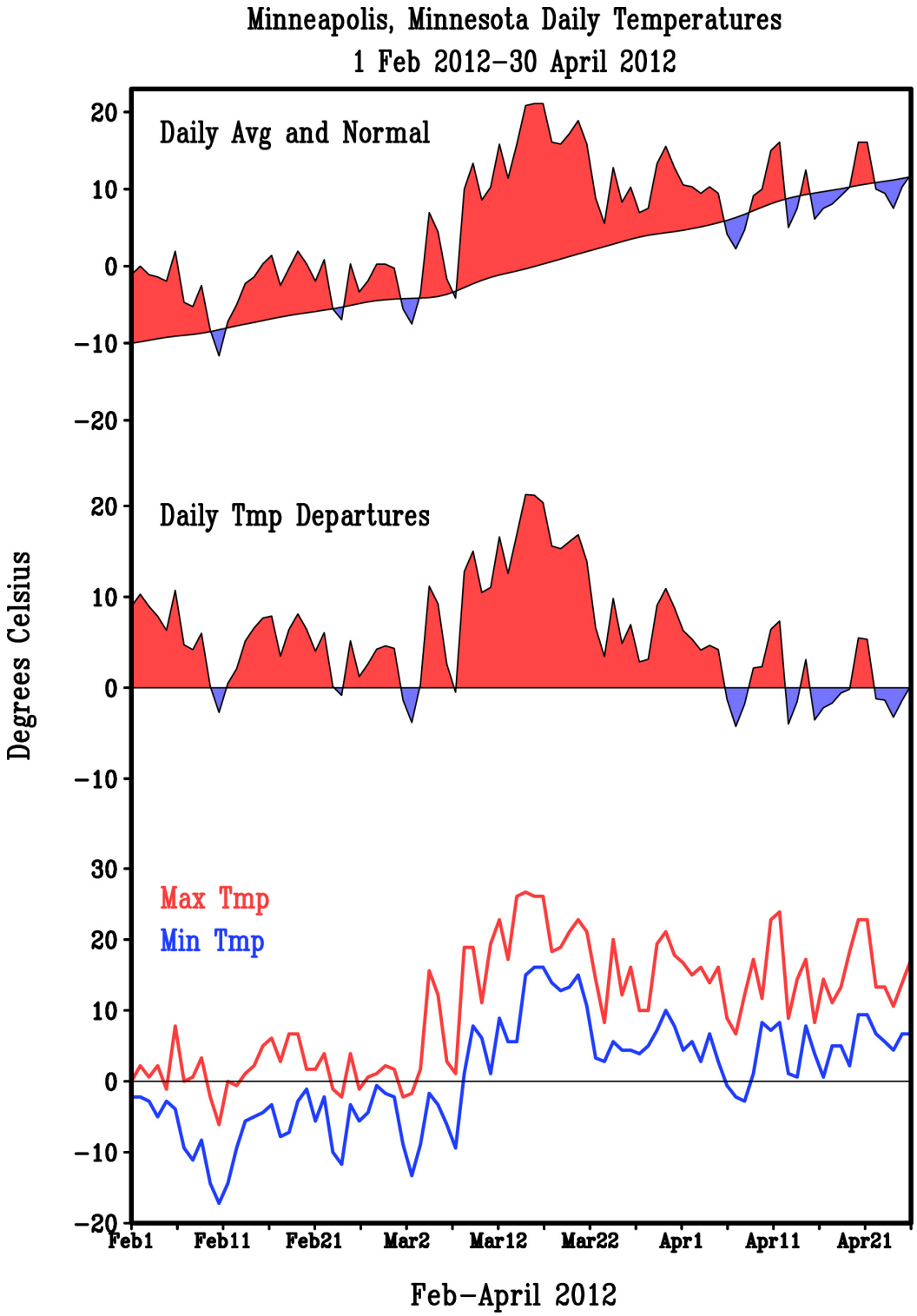

Figure 3. Daily-average temperatures (top), daily departures (middle), and maximum and minimum temperatures (bottom) for Minneapolis, MN for February to April 2012 (°C). Temperature data are from the Global Daily Climatology Network.

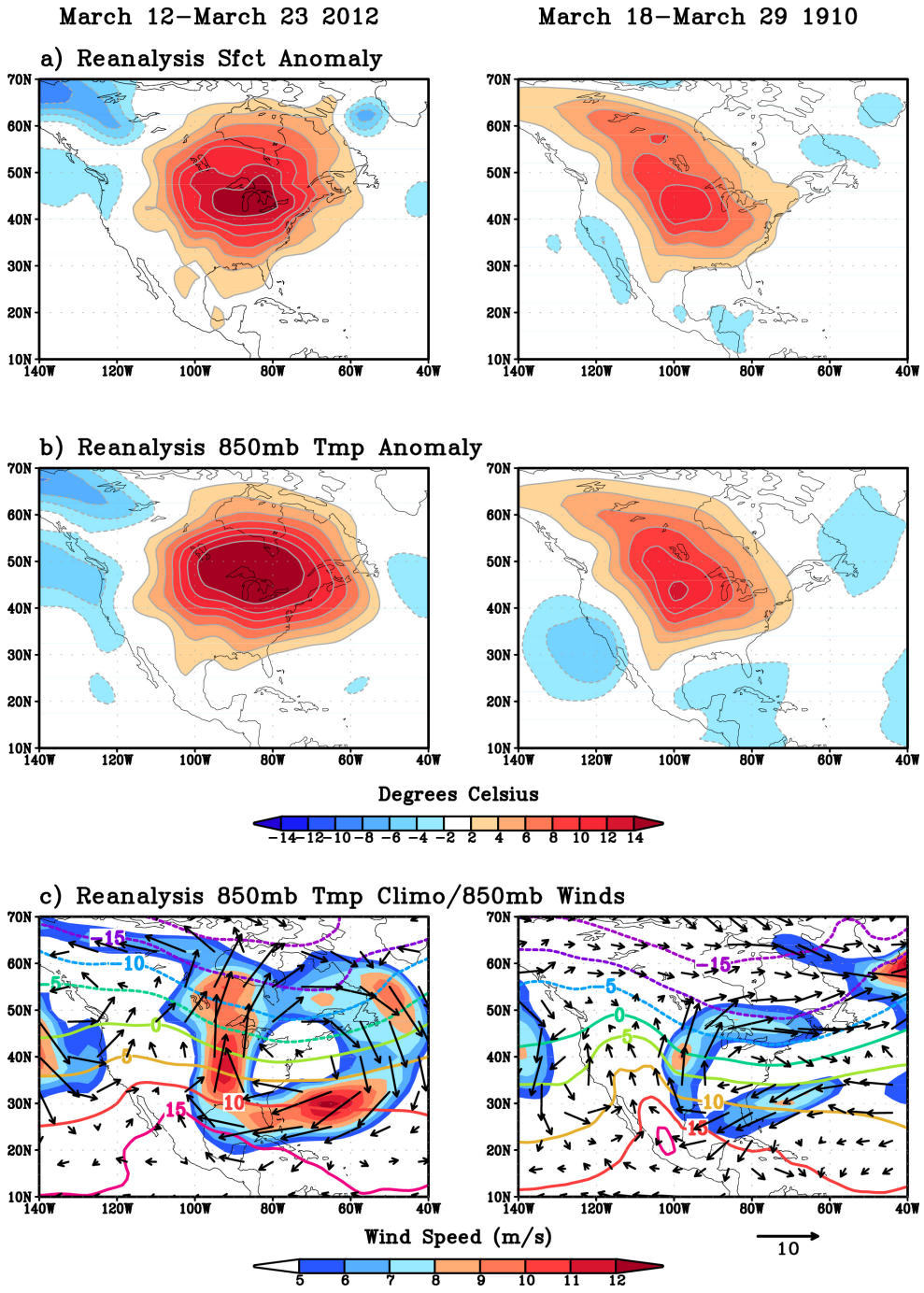

Figure 4. Left side panels: 12-23 March 2012 time-mean a) Surface temperature anomalies (ºC), b) 850 hPa temperature anomalies (ºC), and 850 hPa vector wind anomalies together with March climatological-mean 850 hPa temperatures (ºC). The right side panels show corresponding maps for 18-29 March 1910. Data for 2012 are derived from the NCEP/NCAR Reanalysis (Kalnay et al. 1996), and for 1910 from the 20th Century Reanalysis Project (Compo et al. 2011).

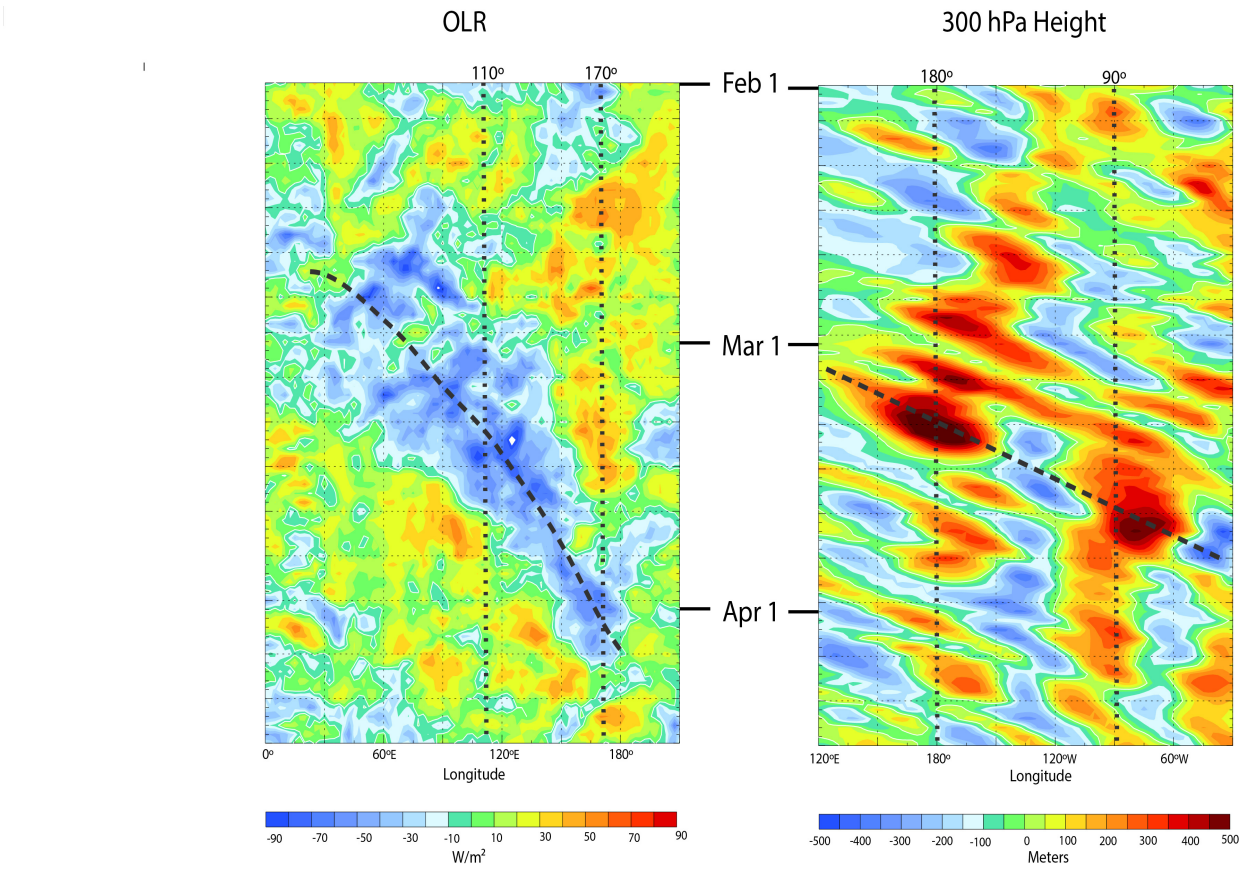

Figure 5. Time-longitude analyses over the period February 1- April 30 2012 of a) OLR anomalies (W m^{-2}) averaged over 5ºN-5ºS extending from West Africa to the east-central Pacific and b) 300 hPa height anomalies (m) for a mid-latitude band (30-50º N) from East Asia to the eastern North Atlantic. The sloped dash lines depict (a) the eastward propagating MJO convective signal, and (b) downstream energy dispersion from the Pacific to the North Atlantic.

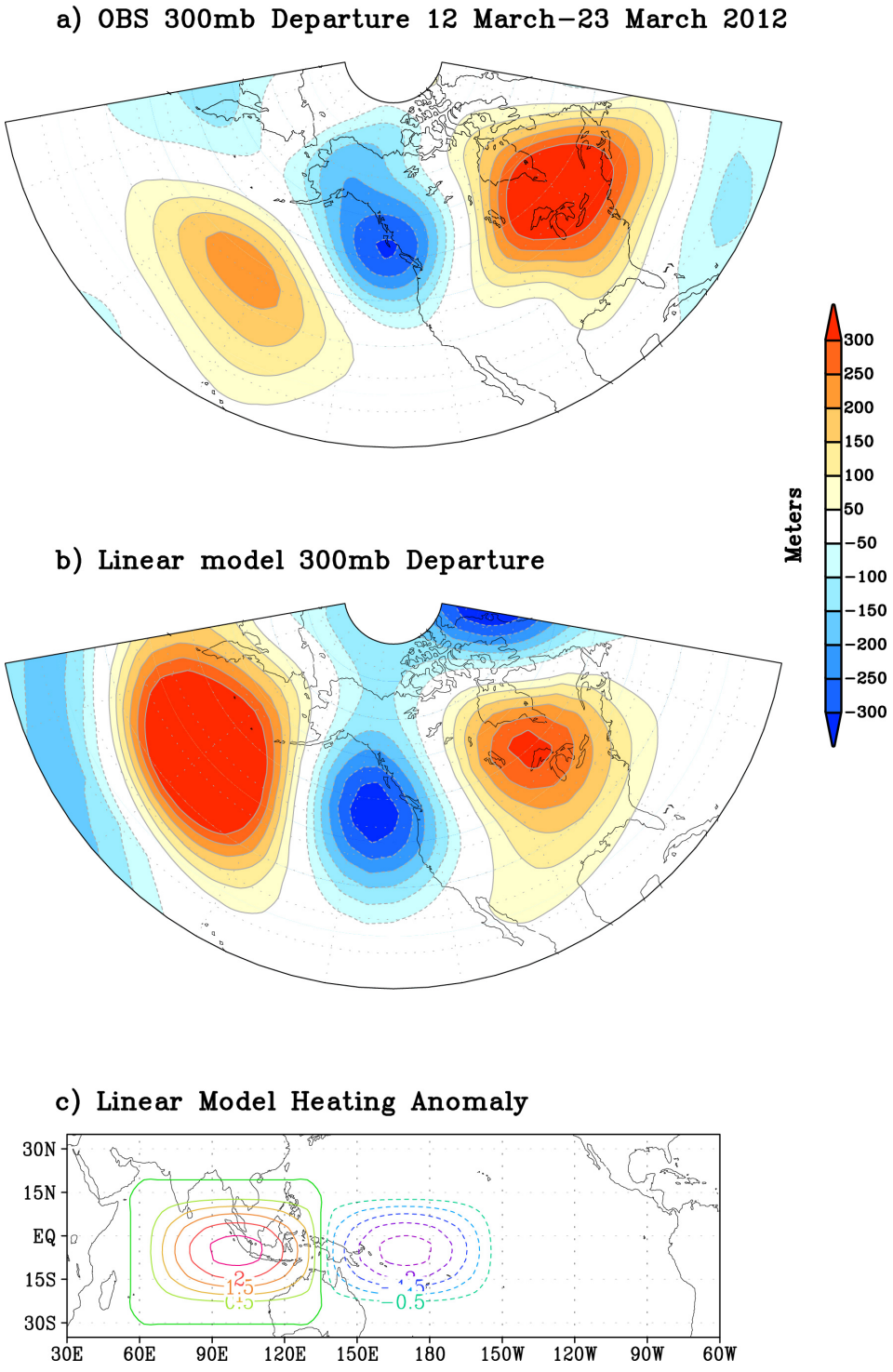

Figure 6. Comparison between observed 300 hPa height anomalies and the response of a Linear Baroclinic Model (LBM) to forcing from tropical diabatic heating anomalies similar to those observed in early March 2012. (a) March 12-23 time-mean 300 hPa height anomalies (m). (b) LBM response to anomalous tropical forcing (m). (c) Idealized diabatic heating pattern used to force the LBM. For further details on the LBM, see Appendix 1.

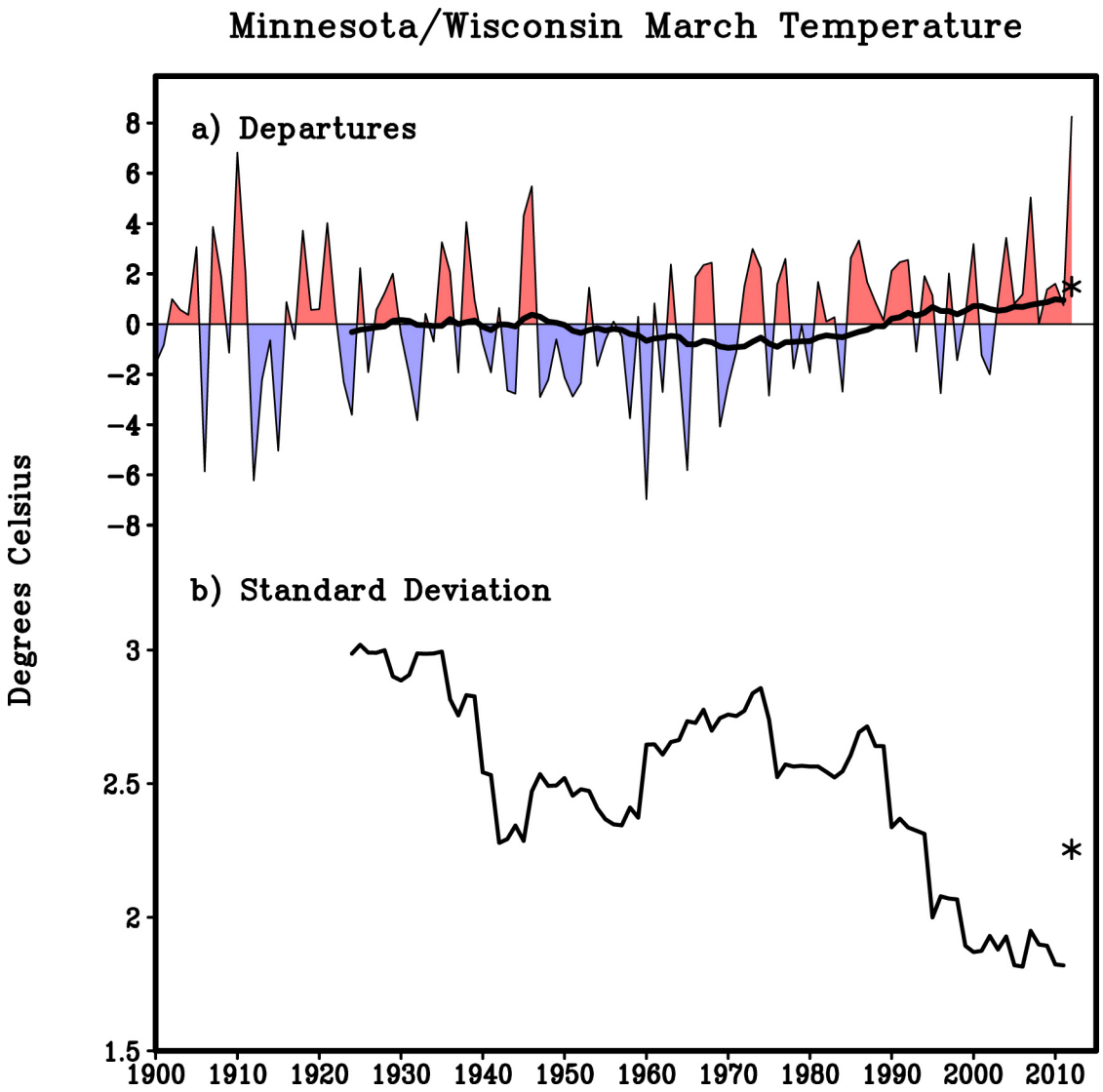

Figure 7. Minnesota-Wisconsin area-average a) March temperature anomaly time series from 1900 to 2012, along with 30-year running mean of this average plotted at the ending year, and b) the standard deviation of the March area-average temperatures about their 30-year running means, plotted at the ending year (°C). From NCDC Climate Division data. Asterisks denote the values of the 30-year mean and standard deviation for 1983-2012.

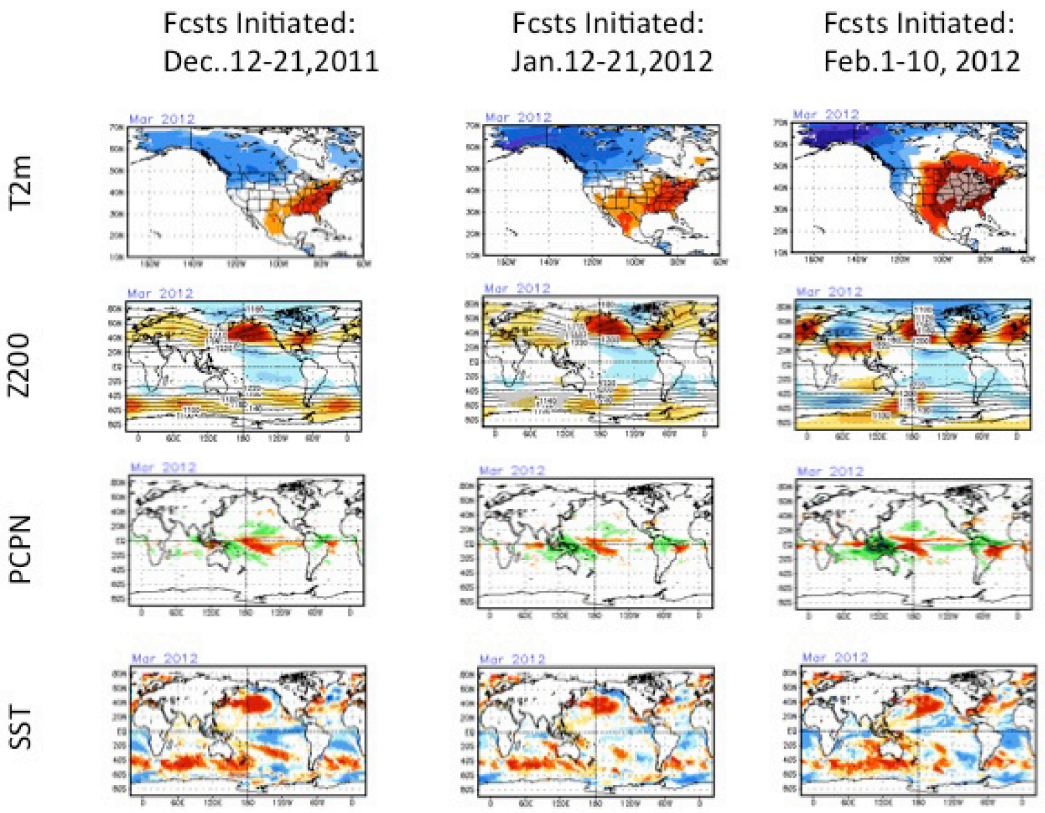

Figure 8. Operational ensemble mean CFSv2 forecasts verifying March 2012 based on initializations during (left) December 12-21 2011, (middle) January 12-12 2012, and (right) February 1-10 2012. Predictions are for (top) surface temperature anomalies (first interval 0.5°C, 1°C intervals thereafter; warm (cold) anomalies in red (blue)), (second row) 200 hPa heights (total field contoured, anomalies shaded every 15m; positive (negative) anomalies in red (blue)), (third row) precipitation anomalies (first interval 1mm/day, 2mm/day intervals thereafter; wet (dry) anomalies in green (red)), and (bottom) sea temperature anomalies (intervals are 0.25, 0.5, 1.0, and 2.0 °C; warm (cold) anomalies in red (blue)). Predictions are made four-times daily, yielding a 40-member ensemble for each 10-day period. All anomalies are relative to CFSv2 lead-time dependent hindcast climatologies for 1982-2010.

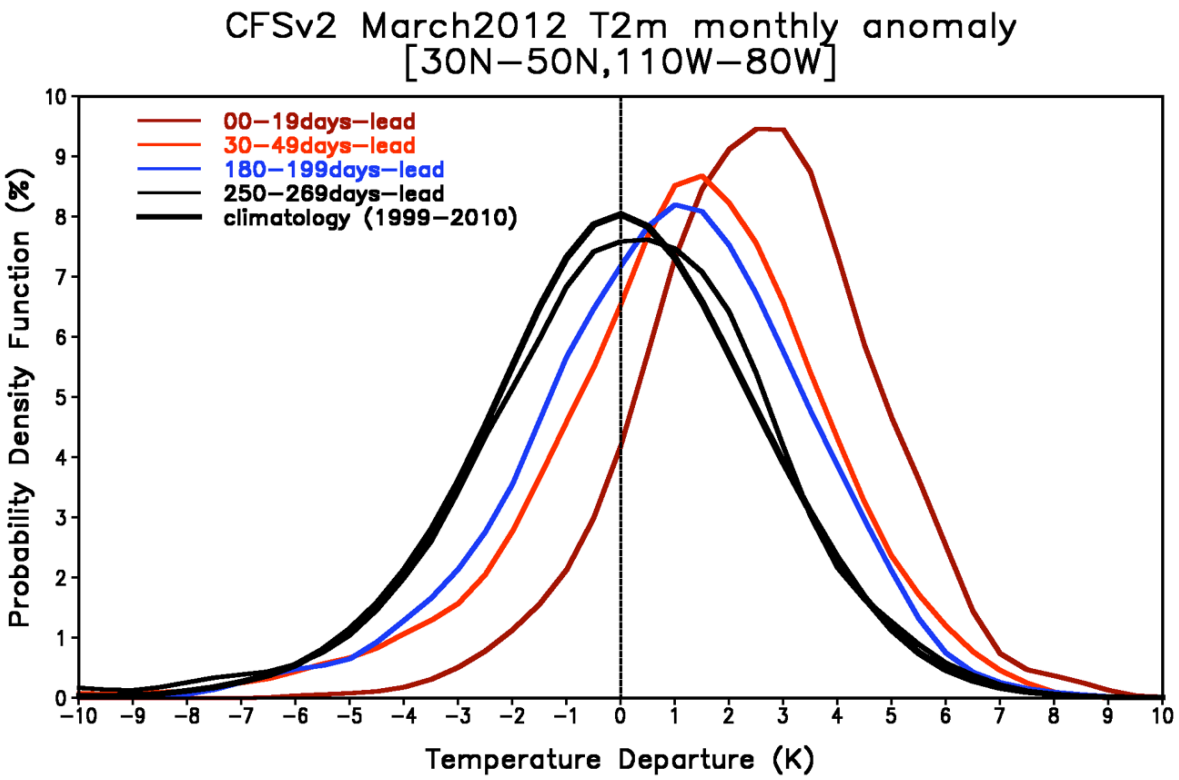

Figure 9. The PDFs of 2-meter air temperature monthly anomalies for March 2012 derived from CFSv2 model predictions at different lead times (thin curves) and for a March climatological distribution of hindcasts (thick black curve). All prediction PDFs are derived from 80-member ensembles, while the climatological PDF is derived from all March hindcasts (retrospective forecasts) up to 6 months in advance over the years 1999-2010 (1728 members). Predictions are averaged for the region 30N-50N, 110W-80W.

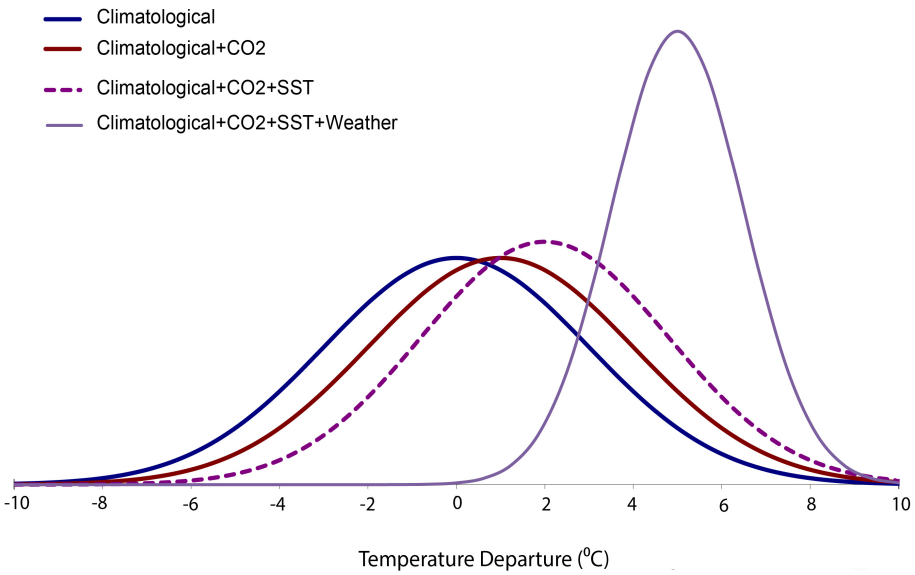

Figure 10. A schematic representation of how predictions for the March 2012 PDF shifted away from the climatological distribution (blue) in response to different factors. These include multi-decadal variations and trends operating on time scales well beyond a season (red), SSTs and other boundary forcings on seasonal time scales (dashed), and the MJO and other phenomena dominated by atmospheric processes on subseasonal-to-daily time scales.

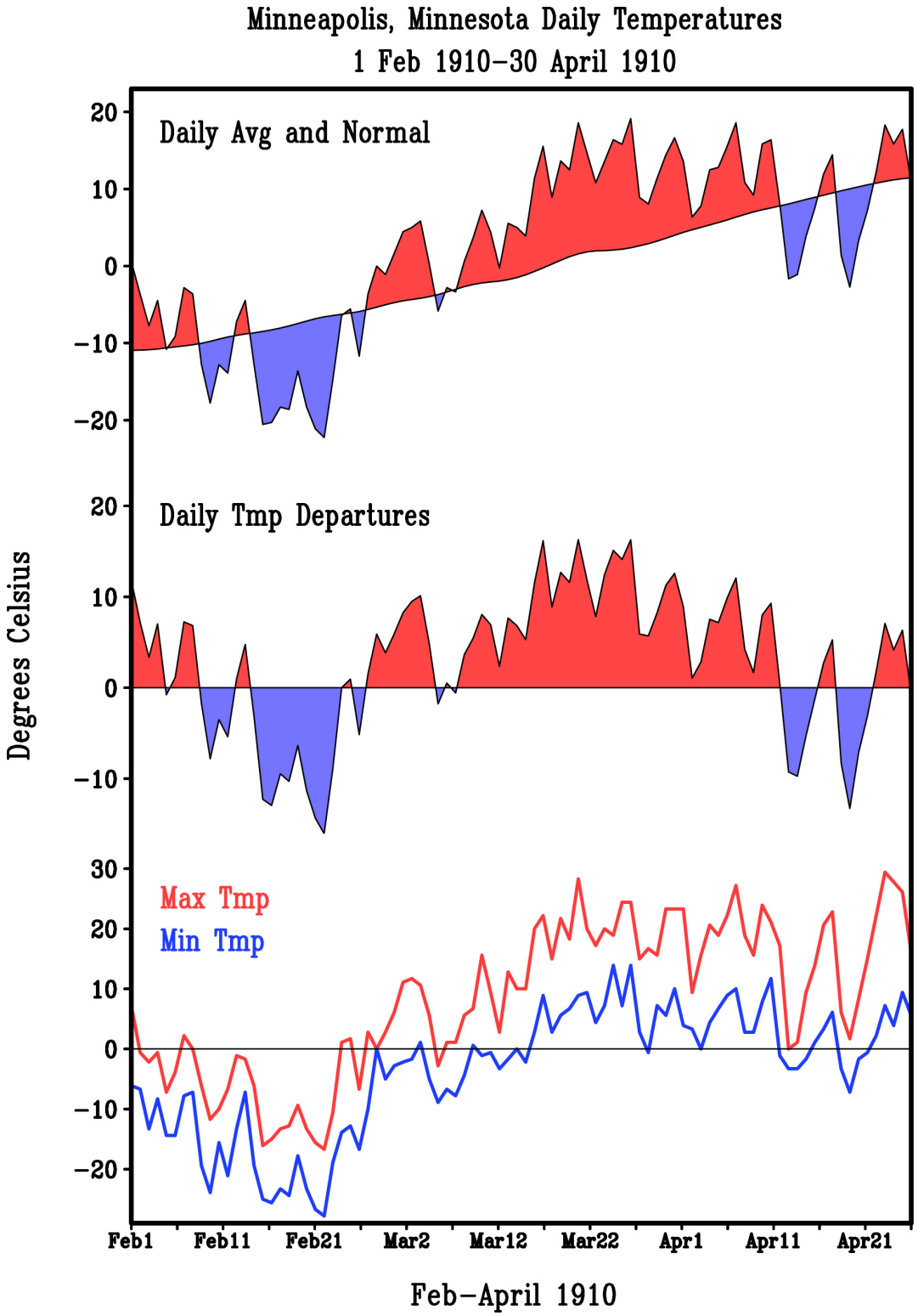

Figure S1. As in Figure 3 for Minneapolis, Minnesota temperature time series for Feb-April 1910.

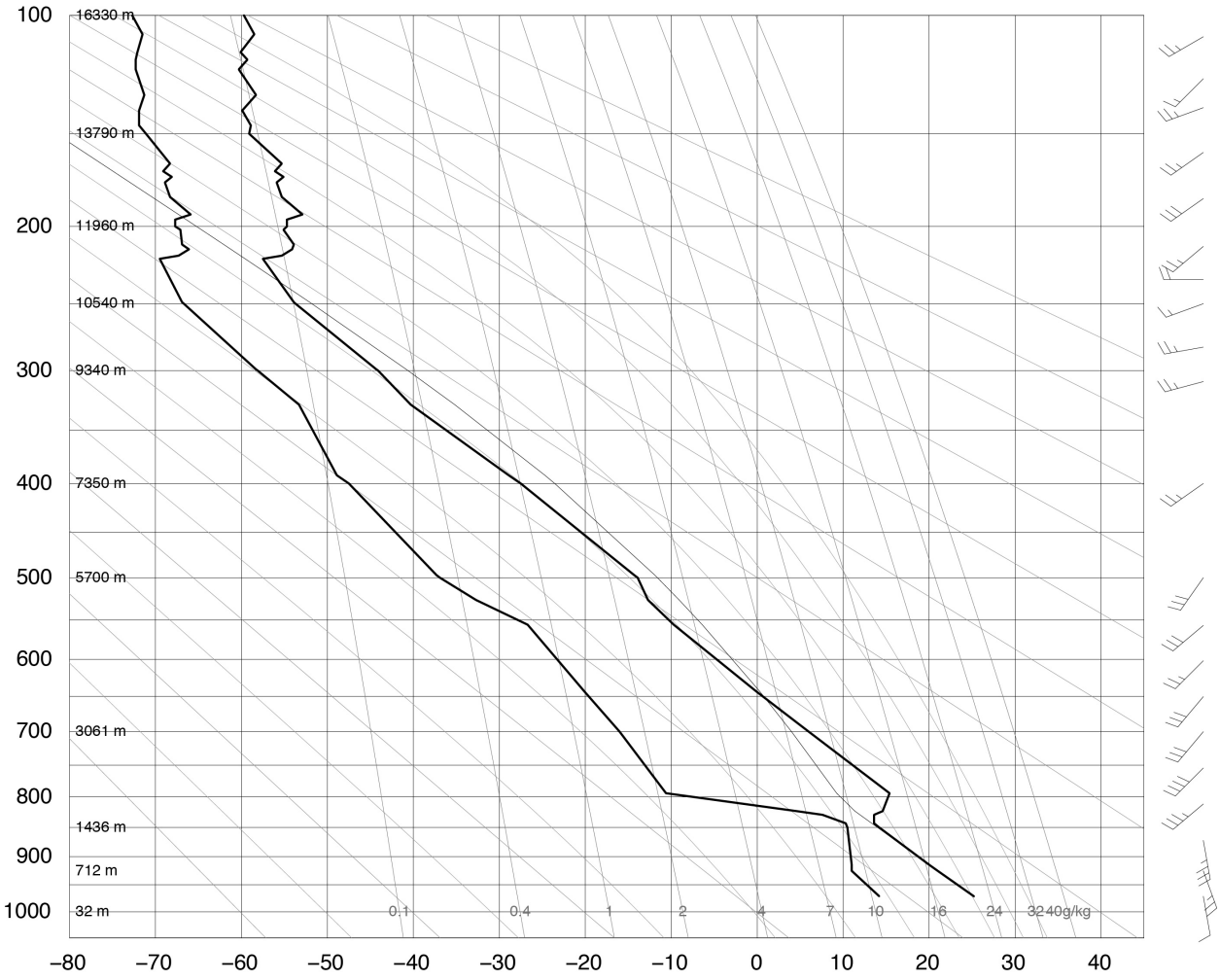

Figure S2. Radiosonde data from the surface to 100 hPa of temperatures and dewpoints (ºC) and winds for Chanhassen (Minneapolis, MPX) on March 19 2012 00Z.

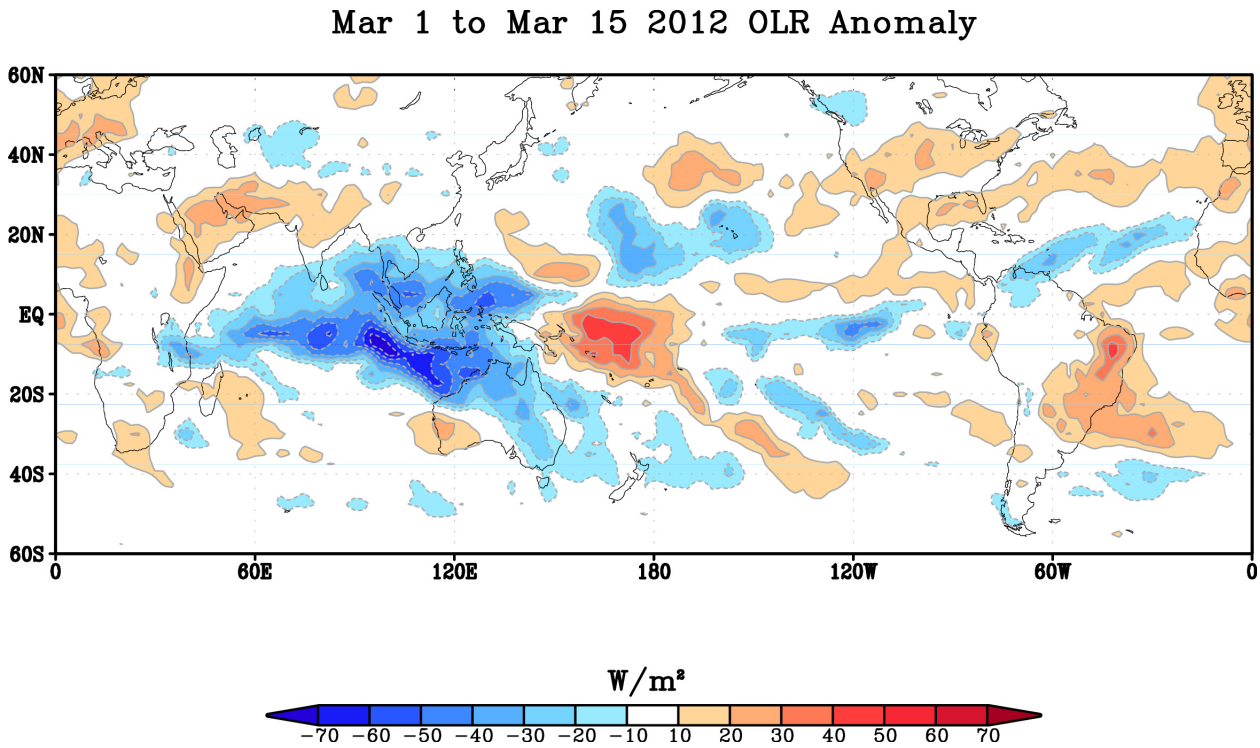

Figure S3. Time-mean OLR over March 1-15 2012 (W m^{-2}). Data source as in Figure 2.

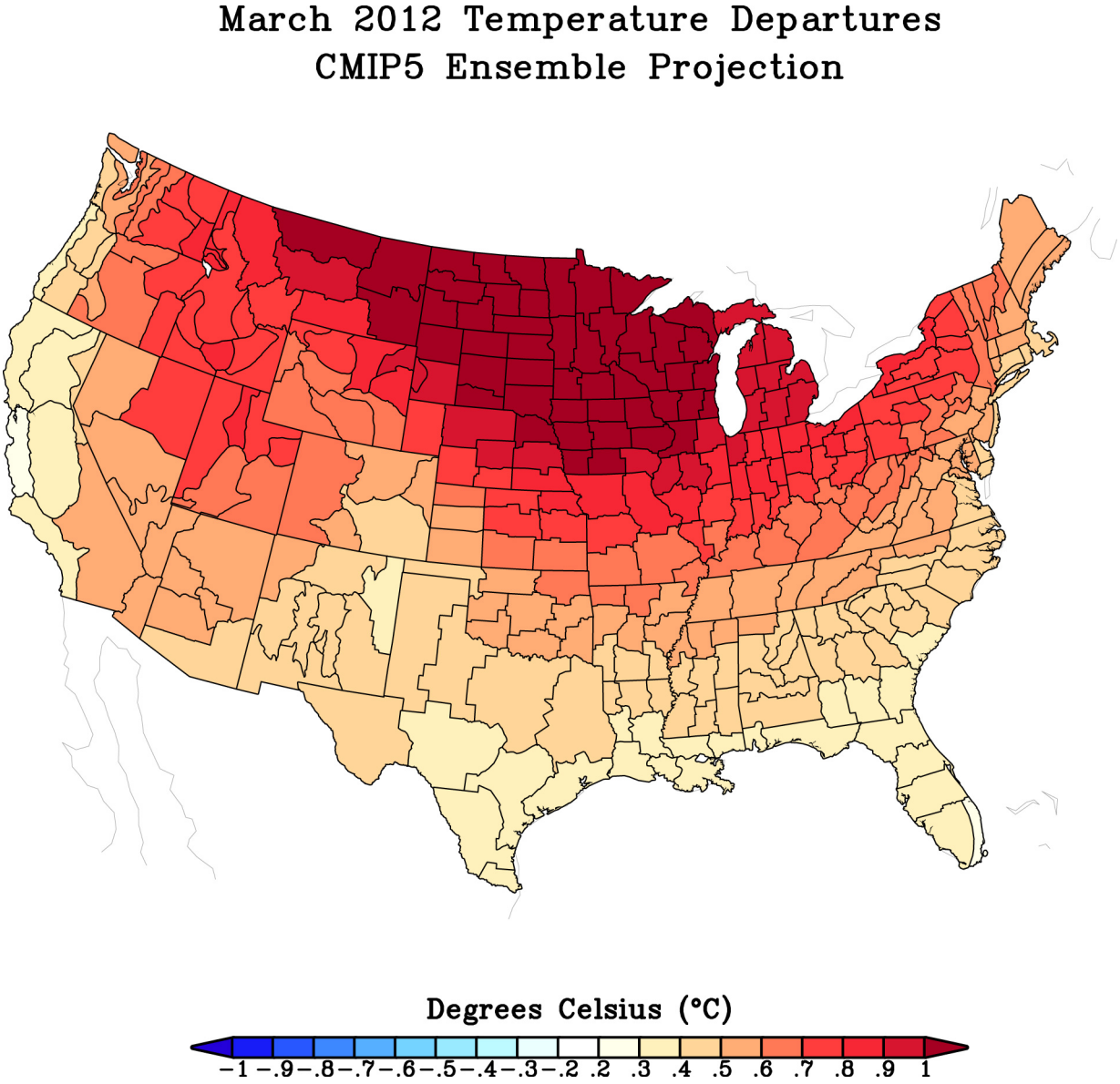

Figure S4. CMIP5 ensemble average of projected March 2012 temperatures anomalies (in ºC relative to model 1981-2010 climatology).

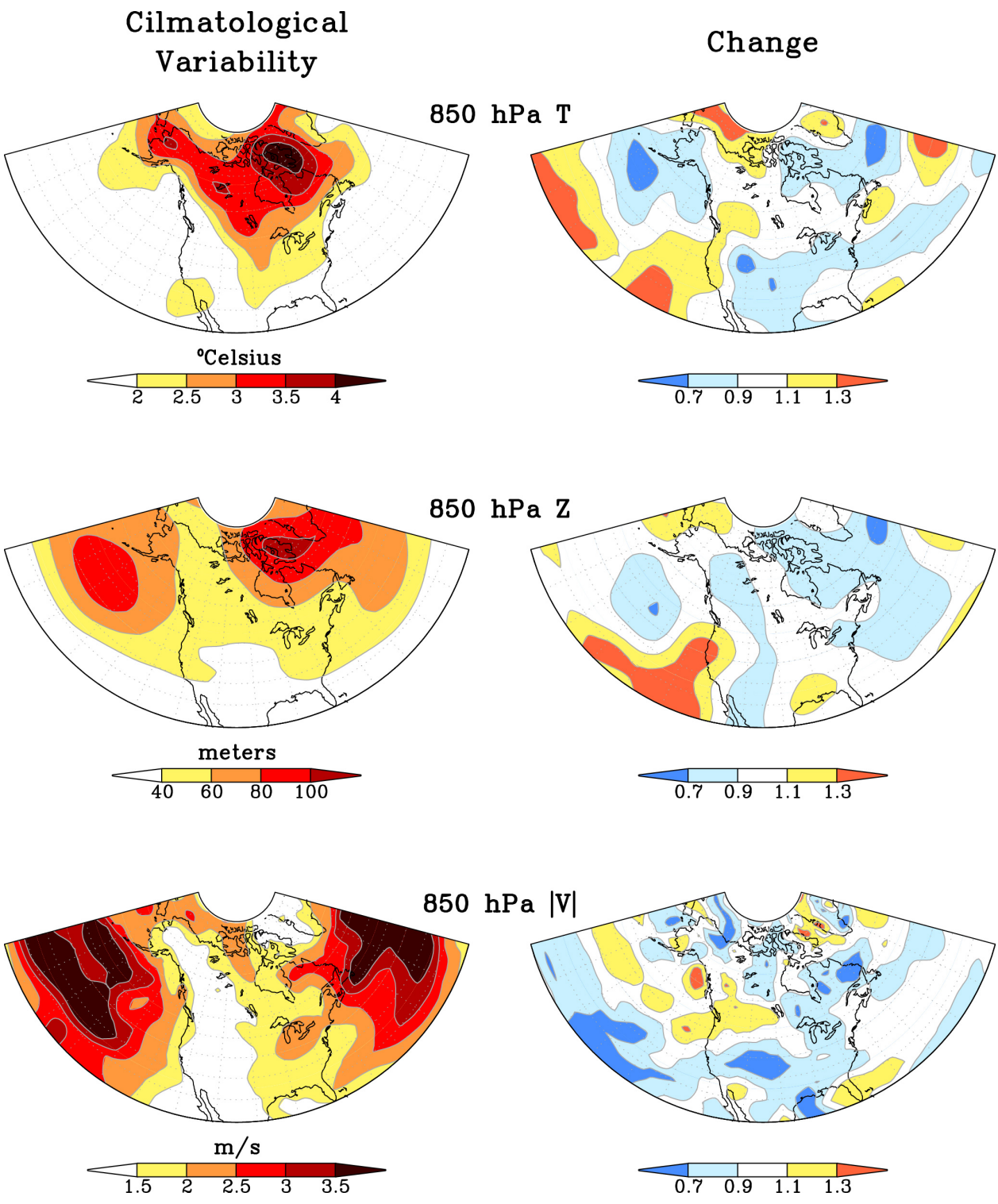

Figure S5. Standard deviation of monthly March 850 hPa temperature (top), 850 hPa geopotential height (middle) and 850 hPa meridional wind speed (bottom) over the base period 1961-1990 (left) and the ratio of standard deviations for 1991-2011 relative to 1961-1990 (right). [Data source: NCEP/NCAR reanalysis].

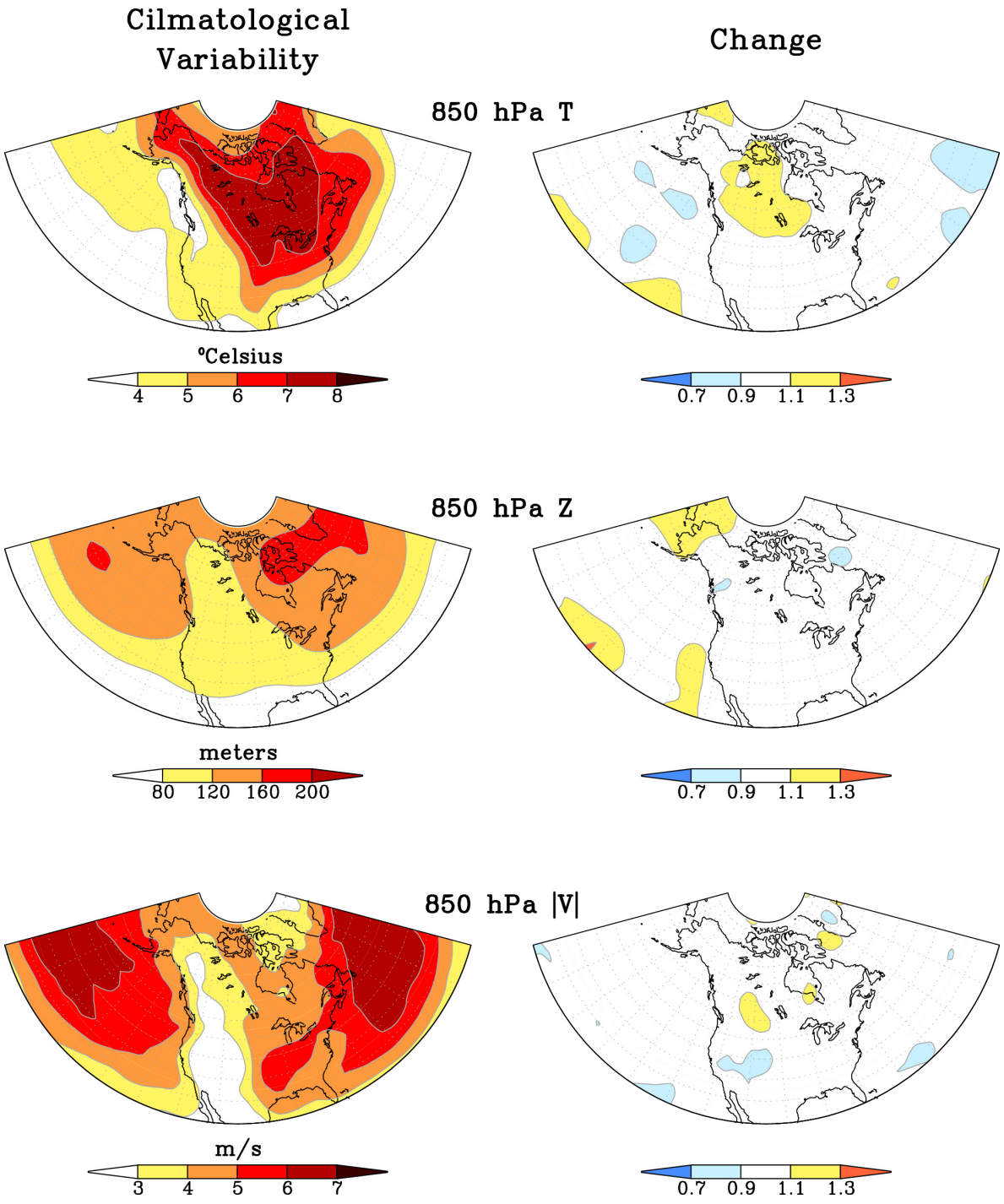

Figure S6. As in Supplementary Figure 5 but for standard deviations of daily temperatures in March (left) for 1961-90 and the ratio of standard deviations for 1991-2011 relative to 1961-90 (right). Contour intervals for the 1961-1990 base period (left panels) are doubled relative to monthly values in Figure S5.